RSC Advances

ROYAL SOCIETY OF CHEMISTRY

www.rsc.org/advances

RSC Advances

RSCPublishing

PAPER

Kinetics of glass transition, negative magnetization and exchange bias effects in $Sm_{1-x}Bi_xCrO_3$

Cite this: DOI: 10.1039/x0xx00000x

Xiao-Long Qian,[a] Jian Kang,[a] Bo Lu,[b] Shi-Xun Cao,[a,c] and Jin-Cang Zhang,[a,b,c,*]

Received 00th January 2014,
Accepted 00th January 2014

DOI: 10.1039/x0xx00000x

www.rsc.org/advances

The dc magnetization and magnetic relaxation studies of polycrystalline sample $Sm_{1-x}Bi_xCrO_3$(x=0, 0.1) show the kinetics of magnetic glass behavior in $SmCrO_3$, the results indicate the frozen antiferromagnetic state is dominative to the glassy transition. The glass transition temperature and the frozen components could be tuned by external fields, and the proportion of the frozen fraction could reach ~53.2% in this system. The doping of Bi in Sm site gives rise to a zero field negative magnetization and the vanishing of glassy behaviors in $Sm_{0.9}Bi_{0.1}CrO_3$. Negative magnetization was found to be strongly dependent on the external field. The spin reorientation transition temperature and the Nèel transition temperature decrease significantly after substitution. The exchange bias effects detected in the magnetization-field isotherm curves at 5 K and 10 K confirm the strong interactions of Sm^{3+}-Cr^{3+} spins in $Sm_{0.9}Bi_{0.1}CrO_3$.

Introduction

Over the years, chromites have been investigated using neutron diffraction, specific heat capacity, Mossbauer, magnetic, and optical measurements[1-8]. Recently the rare earth orthochromites continue to draw attention for their various magnetic properties, such as spin-reorientation transitions, exchange bias, spin frustration and other highlights[9,10]. It has been observed that there exist different spin magnetic structures in the temperature range between the spin reorientation transition temperature(T_{SR}) and Nèel transition temperature(T_N) [11,12]. According to the Bertaut notation, three G-type antiferromagnetic (AFM) configurations are studied in $RCrO_3$: Γ_1 (A_x, G_y, C_z), Γ_2 (F_x, C_y, G_z) and Γ_4 (G_x, A_y, F_z)[5]. The first configuration does not allow weak ferromagnetism, but the second and third have weak ferromagnetism along the x and z directions, respectively. Normally, if the R ion is nonmagnetic, the ground state of $RCrO_3$ remains weakly ferromagnetic with the configuration Γ_4. If the R ion is magnetic, the high-temperature magnetic structure can be Γ_4 or Γ_2 depending upon the R ion[13].

Up to now, although numerous researches have been carried out, the underlying mechanism of glass transition remains a puzzle[14-18]. The glass formes when kinetics is arrested below a glass transformation temperature (T_g) preserving the high-temperature structure, while the liquid-solid transformation is avoided above the crystallization temperature (T_C). If heterogeneous nucleation is inhibited by the absence of nucleation seeds, then the supercooled state will persist below T_C, and homogeneous nucleation takes place only when the free energy barrier reduces to ~kT in the neighborhood of the supercooling limit T^*[19]. T_g has been defined in previous studies as the temperature where the field-cooled cooling curve starts flattening out without touching zero-field cooling curve, and T^* are defined as the temperature where the field-cooled cooling curve meets with the zero-field cooled curve while cooling down. More rigorously, T_g is the temperature where the characteristic relaxation time crosses the typical experimental time involved in measurements. The recently discovered 'magnetic glasses' reveal interesting kinetic behaviors as reported in several studies[20-22]. The magnetic glass normally experiences a viscous retardation of nucleation and crystallization in their supercooled state. The evidences of a magnetic glassy behavior are investigated in some ternary alloy system, such as $Ni_{50}Mn_{50-x}In_x$, $Ce(Fe_{0.96}Ru_{0.04})_2$ and so on[23,24]. Those materials show the presence of significant thermomagnetic irreversibility correlated with large divergence between the field-cooled cooling (FCC) and field-cooled warming (FCW) data.

The phenomenon of exchange bias (EB) was firstly discovered in the core/shell nanoparticles consisting of ferromagnetic (FM) Co core and antiferromagnetic (AFM) CoO shell[25]. Ever since, the EB associated with the exchange coupling between FM and AFM interface has attracted much attention due to its potential applications[26,27]. In the last few years, the phenomenon of NM and EB was reported extensively in orthochromites [28-30] and orthomanganites[31,32].

The aim of the present paper is to report the magnetic glassy properties of $Sm_{1-x}Bi_xCrO_3$(x=0, 0.1). Firstly the study of spin reorientation(SR) transition and magnetic glass(MG) transitions by dc magnetization as a function of temperature were discussed in $SmCrO_3$. The behaviors of magnetization curves on cooling and warming cycling exhibits the existence of frozen AFM components. Then the kinetics of glassy transitions is examined by the magnetic relaxation measurement and also in a quantitative method by evaluating the activation energy. Finally, the negative magnetization(NM) and the vanishing of glassy behaviors were detected in $Sm_{0.9}Bi_{0.1}CrO_3$. The isothermal hysteresis loops reveal the

existence of exchange bias(EB) in $Sm_{0.9}Bi_{0.1}CrO_3$, the potential mechanism and explanation for NM and EB in this system are also discussed.

Experimental

The samples were prepared by the standard solid-state reaction. The starting materials Sm_2O_3, Cr_2O_3 (Bi_2O_3 for doped sample) were grinded up together stoichiometric proportions for 3 h in an agate mortar followed by reaction in an alumina crucible at 900° C for 12 h. The powder thus obtained was then reground, pelletized, placed in the crucible, and reacted at 900° C for 24 h. The last step was repeated once with reaction at 900° C for 24 h followed by slow cooling in air. The crystallinity and microstructure of the samples were checked by X-ray diffraction with a scanning step of 0.02° and 2θ from 10° to 90°. The surface morphology was observed by scanning electron microscopy (SEM). The elemental analysis of the samples was done using energy dispersive spectroscopy (EDS).

The dc magnetization measurements were performed with the commercial physical property measurement system (PPMS, Quantum Design). Magnetization temperature (M-T) curves were measured from 5 K to 300 K in the zero-field cooling (ZFC), the field-cooled cooling (FCC) and the field-cooled warming (FCW) modes. In the ZFC measurements, the sample was cooled from room temperature to 5 K in a zero magnetic field, then a field was applied at 5 K, and the M_{ZFC} was measured in the warming cycle, then the M_{FCC} was performed in the cooling cycle and the M_{FCW} in the warming cycle under the same fixed magnetic field. In this experiment, the cooling and warming rate is 1.5 K/min. The magnetization-field (M-H) isotherm curves were measured within H = ±70 KOe at different temperatures. For the M-H curves, before each run, the sample was heated above the T_N and cooled to the measuring temperature under zero fields in order to ensure a perfect demagnetization. The M-T results are with good reproducibility based on our careful and repeated measurements.

Results and discussion

X-Ray diffraction patterns of polycrystalline samples of $SmCrO_3$ and $Sm_{0.9}Bi_{0.1}CrO_3$ are presented in Fig. 1. It shows all samples have a single phase pattern. The lattice parameters calculated from the present XRD data are a=5.372Å, b=5.507Å, c=7.649Å, V=226.3 $Å^3$ for $SmCrO_3$, and a=5.365Å, b=5.498Å, c=7.672Å, V=226.3 $Å^3$ for $Sm_{0.9}Bi_{0.1}CrO_3$, the results are close to the previous report[8]. Upon doping, the XRD analysis indicates no appreciable structural changes as one can see both the number of diffraction peaks and their relative intensities do not undergo substantial change. The reaction products can be assigned to the perovskite structure with *Pbnm* space group and the samples crystallize in single phase.

The representative SEM micrographs of $SmCrO_3$ and $Sm_{0.9}Bi_{0.1}CrO_3$ are shown in Fig. 1(b), respectively. It can be seen that the particle size of $Sm_{0.9}Bi_{0.1}CrO_3$ is smaller and the particles are more agglomerated after substitution. The difference between the two microstructures indicates the underlying difference on their properties. The chemical compositions are illustrated by EDS analysis as shown in Table.1. The presence of Bi is detected in the doped sample and the analyses support that the Bi atoms are successfully doped in $SmCrO_3$.

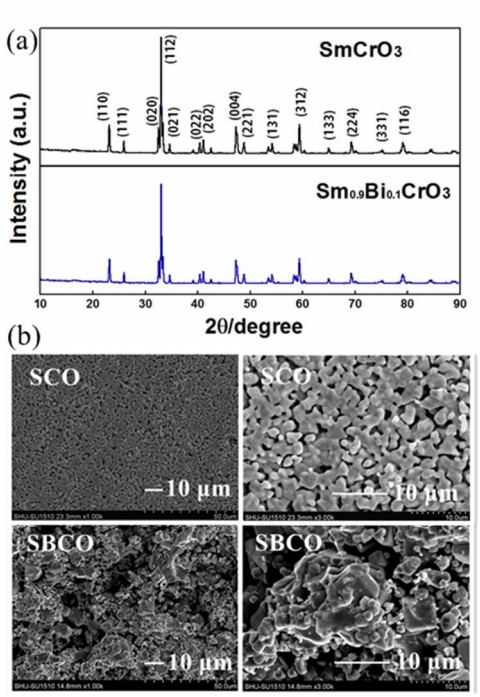

Fig. 1 (a)Room temperature X-ray diffraction patterns for $SmCrO_3$ and $Sm_{0.9}Bi_{0.1}CrO_3$. (b)Scanning electron micrographs of $SmCrO_3$ and $Sm_{0.9}Bi_{0.1}CrO_3$.

Table 1 The chemical composition of studied samples based on the EDS analysis.

	SCO			SBCO			
Element	O	Cr	Sm	O	Cr	Bi	Sm
Wt.(%)	20.22	19.16	60.62	18.93	18.33	9.46	53.28
At.(%)	62.09	18.10	19.81	61.14	18.21	2.34	18.31

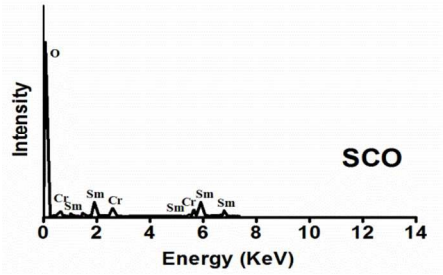

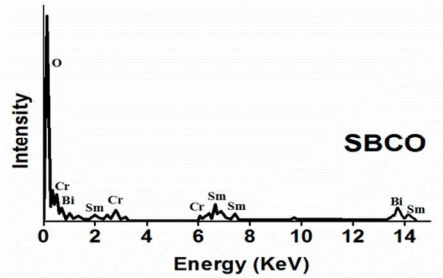

Fig. 2(a) and (b) illustrates ZFC, FCC and FCW magnetization data for $SmCrO_3$ under H = 100 Oe. The giant divergence between FCC and FCW data indicates a glassy arrest of kinetics in the process of AFM-FM phase transition[22], which could be judged as a magnetic glassy transition. The magnetization curves increase between 25 K and 40 K, corresponding to the magnetic phase transition

($\Gamma_2 \rightarrow \Gamma_4$) happened in $SmCrO_3$. In order to acquire more comprehension on the mechanism of glass transition, we studied the kinetically cycling of glass transition in the phase transition temperature range. As for the dM/dT variation is broad and goes much lower than 36 K under different external fields, we only studied the limiting cooling temperature for $SmCrO_3$ under H = 100 Oe. As showed in Fig. 2(c), the sample was cooled from 300 K to 33 K directly, and then was warmed from 33 K to 40 K and cooled back to 30 K, the magnetization results shows that FCW path(a→b) and FCW path(b→c) drops down and separated from the initial FCC curve. After that, the sample was warmed up again to 40 K(c→d), this time the FCW data drops down more than the last path. Then it was cooled down to 30 K(d→c), and warmed up back to 300 K, in this case, the FCW data(30 K - 300 K) follows the last FCW path(30 K - 40 K). This result reveals a thorough glass transition occurred after the sample was cooled down to the limiting cooling temperature. Specifically, in this glass transition process, the FCC data appears larger than that of FCW, the glassy arrested FM-AFM magnetic phase fraction devitrifies in the FCW mode, and the system tries to approach the equilibrium AFM phase, resulting in a decrease of magnetization. It is worthwhile to notice that this magnetic glassy transition is correlated to the thermomagnetic irreversibility showed in FCC and FCW data. We are fully convinced that the magnetic state in this system attains a configuration consisting of frozen AFM component in an untransformed non-equilibrium AFM matrix.

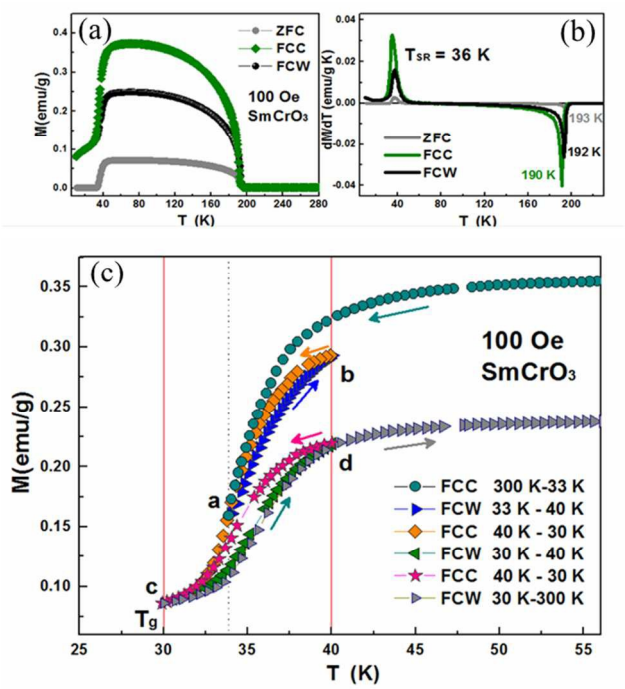

Fig. 2. (a)ZFC, FCC and FCW magnetization curves of $SmCrO_3$ under H = 100 Oe. (b)Temperature dependent dM/dT plots for ZFC, FCC and FCW mode of $SmCrO_3$ under H = 100 Oe. (c)Experimental cycling in the transition temperature range, the sample was cooled down to the 33 K on the FCC path, then the FCW and FCC data were measured along various paths.

Fig. 3(a) shows the FCC and FCW curves for $SmCrO_3$ under different external field. Based on the study in Ref. [20], the onset of glass transformation can be defined as the temperature (T_g) where the FCC curve starts flattening out. In Fig. 3, the flattening out point of FCC data is exactly corresponding to the bifurcation point between FCC and FCW data, and the glass transition temperatures are marked. We found that the magnetic glass transition temperature T_g increased from 25 K to 42 K with the external field changing from 50 Oe to 1000 Oe. The starting glass transition temperature point increased because the $\Gamma_4 \leftrightarrow \Gamma_2$ phase transition was repressed and this glass transition would disappear under the sufficient large external field.

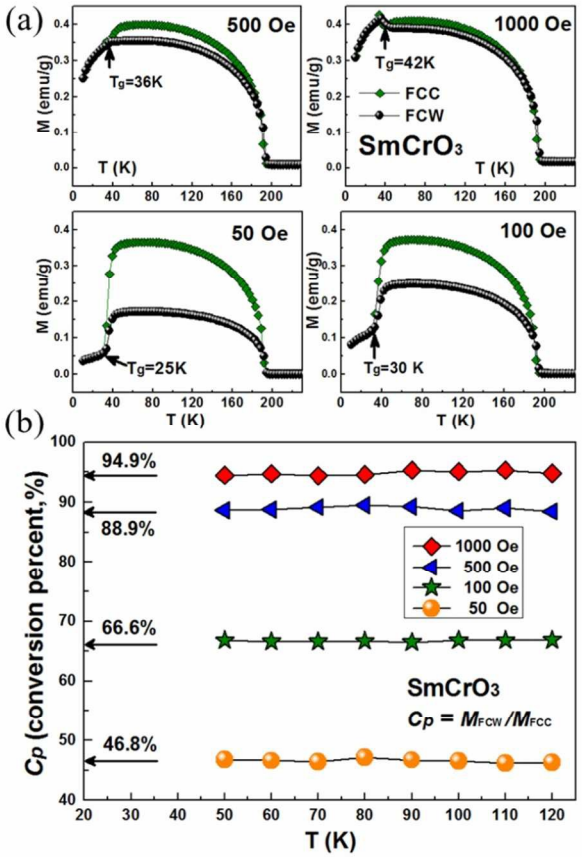

Fig. 3 (a)The FCC and FCW curves for SmCrO3 under external field H = 50, 100, 500, 1000 Oe. The glass transition temperature T_g is marked under various external field. (b) The temperature dependence of the value of *Cp* (conversion percent, $Cp=M_{FCW}/M_{FCC}$) under different external fields after the calculation by curve fitting. The data show the *Cp* in the temperature range from 50 K to 120 K, the arithmetic mean values of *Cp* are stated on the left side. The error bar of the fitting is ≈0.2%.

Here we defined a conversion percent value, C_p, to represent the value of M_{FCW} /M_{FCC} collected at different temperature points. C_p can be regarded as a degree index to trace the phase transitions(FM→AFM) in the FCW path compared to the phase transitions(AFM→FM) in the FCC path, and 1 - C_p is exactly corresponding to the frozen AFM fractions. As shown in Fig. 3(b), the values of C_p are nearly constant in a large temperature range, the mean value we obtained is 46.8%, 66.6%, 88.9% and 94.9% under the external field H = 50, 100, 500, 1000 Oe, respectively. As for a polycrystalline sample, once the FM→AFM phase transitions finished, there exist some frozen AFM fractions in the magnetic domains that could not attend the AFM→FM phase transition. However, the external magnetic field could restrain the magnetic phase transition and tune the component of the frozen AFM phase(from 53.2% under 50 Oe to 5.1% under 1000 Oe).

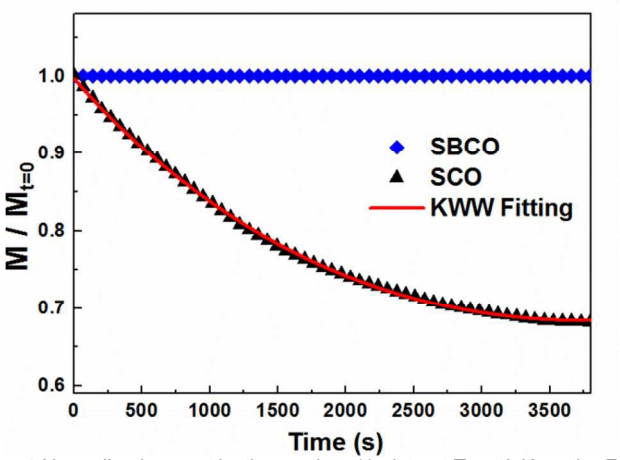

Fig. 4 Normalized magnetization vs time (t) plots at T = 40 K on the FCC path for SCO and SBCO samples. The applied field is 100 Oe. M is normalized with respect to the initial M_0 obtained after 1 s of stabilizing. The solid line represents the fitting with KWW stretched exponential function with α = 0.42. The error bar of the fitting is ≈0.5%.

In order to study the evolution of the arrested glassy state, we measured magnetization as a function of time at 40 K. For measurement at each temperature, the samples were cooled in a magnetic field of H = 100 Oe from T = 300 K to T = 40 K. The magnetic field was then isothermally reduced to zero at T=40 K, following which, the samples were warmed to the measurement temperature and magnetization was measured as a function of time for 60 min. Fig. 4 shows the evolution of M after it is normalized to the respective values of M at t = 0. It is seen that the $SmCrO_3$ show strong relaxation in magnetization while no relaxation was found in $Sm_{0.9}Bi_{0.1}CrO_3$. The M-t data of SCO can be fitted with Kohlrausch-Williams-Watt(KWW) stretched exponential function,

$$\Phi(t) \propto \exp[-(t/\tau)^{\alpha}] \quad (1)$$

where τ is the characteristic relaxation time and α is a shape parameter. This behavior in SCO is typical of what has been observed in many glass formers in the T regime of glass formation[21]. Further, the kinetics of the glass transition could be analyzed by the modified Kissinger equation, and the activation energy (E) can be determined using the following expression

$$\frac{d \ln (\beta/T_g^2)}{d (1/T_g)} = -\frac{E}{R} \quad (2)$$

where R is the ideal gas constant and β is the heating rate[18]. The activation energy calculated using this method is ~506 KJ/mol in SCO. It should be mentioned that the Kissinger models assume that the activation energy is constant throughout the transformation region and therefore it would produce single value of the activation energy for the entire transition process. Here in our study, since the magnetic field takes control of the T_g, the obtained active energy is highly magnetic related.

In $RCrO_3$, canted Cr^{3+} spin induces a magnetic field on the R^{3+} site which leads to the alignment of R^{3+} towards the induced field below T_N, which is large as compared to H_{ext}. Assuming R^{3+} spins follow the Curie-Weiss law, then the average moment(μ_{av}) is the sum of the canted Cr^{3+} spin and R^{3+} spin moments below T_N, which could be explained by the following equation. Here μ_{Cr} and μ_R is the magnetic moment of the Cr^{3+} and R^{3+} ion, respectively.

$$\mu_{av} = \mu_{Cr} + \mu_R \quad (3)$$

If the induced field is larger than the applied field, the second term in this equation becomes greater and hence the net magnetization goes to a negative value. With an increase of the applied field, the first term becomes larger which results in a positive magnetization value. Fig. 5 shows the M-T curves for $Sm_{0.9}Bi_{0.1}CrO_3$ under ZFC, FCC and FCW modes at varying H_{ext} (100 Oe, 1000 Oe, 5000 Oe). The remarkable NM is observed in M_{ZFC}-T curves for H_{ext} = 100 Oe with minimum magnetization ~ -0.17 emu/g. The spin reorientation transition temperature and Nèel transition temperature decrease significantly after substitution, for example, as illustrated in Fig. 4(a). It is noteworthy that the glass transition disappears as no divergence between FCC and FCW curves are found. More than that, the magnetic moment also increases substantially.

NM effect observed in $Sm_{0.9}Bi_{0.1}CrO_3$ is quite an interesting phenomenon and an explanation could be given by the temperature and field dependent interplay between Sm^{3+}-Cr^{3+} spins. NM in orthochromites is mainly due to the antiparallel coupling between R^{3+}-Cr^{3+} spin sublattices[33,34]. After substitution, the interactions between Sm^{3+}-Cr^{3+} spins would induce an internal field in this system. We suggest that the AFM coupling between Sm^{3+} and the canted Cr^{3+} moments dominates over the H_{ext} and leads to the anti-parallel alignment of Sm^{3+} moments with respect to the Cr^{3+} spins. Similar models have successfully explained the NM behavior in $GdCrO_3$ and $DyCrO_3$[35,36].

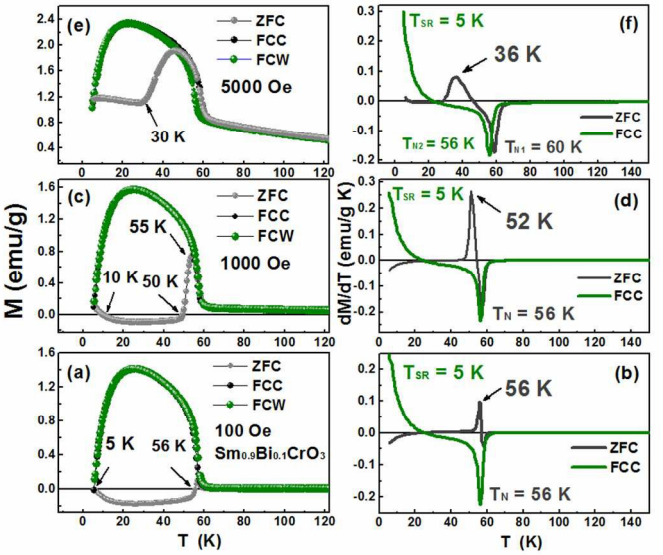

Fig. 5 ZFC, FCC and FCW magnetization curves for $Sm_{0.9}Bi_{0.1}CrO_3$ under H = 100 Oe, 1000 Oe, and 5000 Oe(a, c, e). The temperature dependent dM/dT plots for ZFC and FCC mode under H = 100 Oe, 1000 Oe, and 5000 Oe(b, d, f).

In Fig. 5(c), when H_{ext} = 1000 Oe, the NM effect still exists but weakens compared to that under 100 Oe, as the internal induced field becomes smaller than the H_{ext} which prevents the opposite alignment of Sm^{3+} with respect to weak FM Cr^{3+} moments. The crossover temperature (T_{cross}) from negative to positive M_{ZFC} changes to 50 K, the temperature range of negative M_{ZFC} also narrows from 10 K to 50 K. However, under higher external field, the applied field is much larger and enough to dominate the induced field on Sm^{3+} spins and thus the M-T curve shows a totally positive M_{ZFC} at 5000 Oe, as illustrated in Fig. 5(e). We suggest that the negative magnetization is mainly due to the interactions between Sm^{3+} and Cr^{3+} ions. Several studies have reported that the Bi^{3+} shows the ferromagnetic properties, we believe the interactions between Bi^{3+} and Cr^{3+} should not be neglected [37-40].

However, the coupling between Sm^{3+} and Cr^{3+} ions are too strong that the Sm-Cr interaction is dominant in this system.

Fig. 6 reveals the magnetization-field (M-H) curves for $Sm_{0.9}Bi_{0.1}CrO_3$ within H = ±70 KOe at different temperatures in ZFC modes. The negative EB was observed under 5 K and 10 K. At temperature ~5 K, the hysteresis loops are linear without saturated tendency, revealing strong AFM components, whereas the typical magnetic hysteresis behavior under 30 K and 40 K discloses the coexistence of AFM and FM phase. The obtained exchange bias field (H_{EB}) is ~2800 Oe under T = 5 K and decreases to ~1100 Oe under T = 10 K. With the temperature rises, the effect of exchange bias disappear under 30 K, 40 K, 60 K and 100 K. Furthermore, it can be seen that coercivity (H_C) suddenly increases as we go from 10 K to 30 K and reaches a maximum of ~8950 Oe and then it decreases to ~5300 Oe under 40 K. The linearity at 60 K and 100 K indicates the paramagnetic behavior in this system as the temperature was raised higher than T_N(~56 K). It is well known that the EB occurs in ferromagnetic (FM) and AFM interfacial systems which decreases with an increase of temperature and vanishes at the Nèel temperature[41]. We proposed that the EB in $Sm_{0.9}Bi_{0.1}CrO_3$ is mainly associated with the orientation of the Sm^{3+} moments with respect to the canted Cr^{3+} components. In interface coupling magnetic systems, the exchange interaction between AFM and FM or Ferrimagnetic (FiM) phase can result in an unidirectional anisotropy, along with the enhanced coercivity and the preferred direction of magnetization, indicating the presence of pinned uncompensated spins[42].

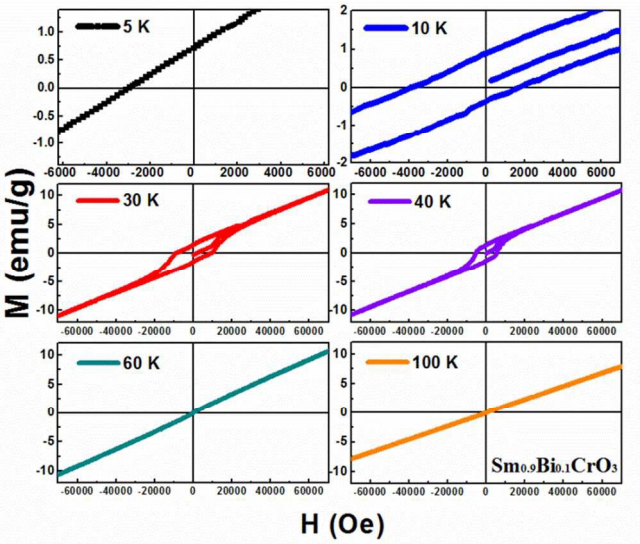

Fig. 6 Isothermal hysteresis loops for $Sm_{0.9}Bi_{0.1}CrO_3$ in ZFC mode measured at 5 K, 10 K, 30 K, 40 K, 60 K and 100 K.

Conclusions

The kinetics of a magnetic glass state in $SmCrO_3$ at low temperature has been shown in the present study. The glassy behavior arises from the kinetic arrest of FM-AFM phase transition due to the frozen AFM fractions. The magnetic glass transition temperature T_g reveals the temperature dependence with external field, while a large magnetic field would clear the frozen fractions and thus the glass transition disappeared. The fitting calculation shows that the highest frozen fraction is about 53.2% in the system under the external field of 50 Oe. The substitution of Bi^{3+} in $SmCrO_3$ leads to remarkable variation on spin reorientation transition temperature and Nèel transition temperature. The negative magnetization was observed in ZFC mode, and the applied magnetic field could tune the negative magnetization. The further study on $Sm_{0.9}Bi_{0.1}CrO_3$ shows the temperature dependent changes in the coercivity and exchange bias. There is strong antiferromagnetic coupling between Sm^{3+} and Cr^{3+} spins below T_N which could be a proper explanation for the NM and EB effect.

Acknowledgements

This work was supported by the National Natural Science Foundation of China (NSFC, Grants No. 11574194, 51372149 and 50932003), Shanghai Institute of Materials Genome (Project No. 14DZ2261200) from the Shanghai Municipal Science and Technology Commission.

Notes and references

[a] *Institute of Materials Genome Initiative (MGI), Shanghai University, Shanghai 200444, China.* Fax/Tel: +86-21-66161146; E-mail: jczhang@shu.edu.cn.

[b] *Laboratory for Microstructures, Shanghai University, 200444, China.*

[c] *College of Science, Shanghai University, Shanghai 200444, China.*

1 E.F. Bertaut, J. Mareschal, *Solid State Commun.* 1967, **5**, 93.
2 C. Veyret, J.B. Ayasse, J. Chaussy, J. Mareschal, J. Sivardiere, J. *Phys. (Paris,* 1970, **31**, 607.
3 M. Eibschutz, L. Homes, J.P. Maita, L.B. Van Uitert, *Solid State Commun.* 1970, **8**, 1815.
4 M.Eibschutz, R.L. Cohen and K.W. West, *Phys. Rev.*, 1969, **178**, 572.
5 F. Bertaut, J. Mareschal, R. Pauthenet, P. Rebouillet, *Bull. Soc. Ceram. A,* 1976, **75**, 44.
6 L. Homes, M. Eibschutz, L.G. Van Uitert, *J. Appl. Phys.,* 1970, **41**, 1184.
7 R. Courths, S. Hiifner, Z. *Phys. B.,* 1975, **22**, 245.
8 S.Kripasindhu, R. L. Martin, J. K.Reza, S.Jeremy, and I.W.Richard, *Chem. Mater.*, 2011, **23**, 48.
9 J.R. Sahu, C.R. Serrao, N. Ray, U.V. Waghmare, C.N.R. Rao, *J. Mater. Chem.*, 2007, **17**, 4931.
10 Z. X. Cheng, X. L. Wang,S. X. Dou,1 H. Kimura and K. Ozawa, *J. Appl. Phys.*, 2010, **107**, 09D905.
11 S. J. Yuan, W. Ren, F. Hong, Y. B. Wang, J. C. Zhang, L. Bellaiche, S. X. Cao, G. Cao, *Phys. Rev. B: Condens. Matter Mater. Phys.*, 2013, **87**, 184405.
12 J. G. Cheng, J. S. Zhou, J. B. Goodenough, Y. T. Su, Y. Sui, Y. Ren, *Phys. Rev. B: Condens. Matter Mater. Phys.*, 2011, **84,** 104415.
13 E.F. Bertaut, G. Bassi, G. Buisson, P. Burlet, J. Chappert, A. Delapalme, J. Mareschal, G. Roult, R. Aleonard, R. Pouthenet, and J.P. Rebouillat, *J. Appl. Phys.* 1966, **37,** 1038.
14 C. A. Angell, K. L. Ngai, G. B. McKenna, P. F. Millan and S. W. Martin, *J. Appl. Phys.*, 2000, **88**, 3113.
15 J. C. Dyre, Rev. *Mod. Phys.*, 2006, **78**, 953.
16 N.R. Cameron and D. C. Sherrington. *J. Mater. Chem.*, 1997, **7**, 11.
17 Y. Nie, X. Ye, Z. Zhou, T. Hao, W. Yang and H. Lu. *RSC Adv.*, 2015, **5**, 17726.
18 H.G. Kissinger, *Anal. Chem.* 1957, **29**, 1702.
19 P.M. Chaikin, T.C. Lubensky, Principles of Condensed Matter Physics, Cambridge University Press, Cambridge, 1994.

20 T. Sarkar, V. Pralong, and B. Raveau, *Phys. Rev. B: Condens. Matter Mater. Phys.*, 2011, **83,** 214428.
21 S.B. Roy, M.K. Chattopadhyay, P. Chaddah, J.D. Moore, G.K. Perkins, L.F. Cohen, K.A. Gschneidner, Jr., and V.K. Pecharsky, *Phys. Rev. B: Condens. Matter Mater. Phys.*, 2006, **74**, 012403.
22 M.K. Chattopadhyay, S.B. Roy, P. Chaddah, *Phys. Rev. B: Condens. Matter Mater. Phys.*, 2005, **72,** 180401R.
23 Y. Sutou, Y. Imano, N. Koeda, T. Omori, R. Kainuma, K. Ishida, K. Oikawa, *Appl. Phys. Lett.*, 2004, **85,** 4358.
24 S.B. Roy, G.K. Perkins, M.K. Chattopadhyay, A.K. Nigam, K.J.S. Sokhey, P. Chaddah, A.D. Caplin, L.F. Cohen, *Phys. Rev. Lett*., 2004, **92,** 147203.
25 W.H. Meiklejohn, C.P. Bean, *Phys. Rev.*, 1956, **102**.
26 K. Yoshii, *Appl. Phys. Lett.*, 2011, **99,** 142501.
27 J. de la Venta, M. Erekhinsky, S. Wang, K.G. West, R. Morales, I.K. Schuller, *Phys. Rev. B: Condens. Matter Mater. Phys.*, 2012, **85,** 134447.
28 A. Jaiswal , R. Das, K. Vivekanand, T. Maityand, P.M. Abraham, S. Adyanthaya and P. Poddar, *J. Appl. Phys*., 2010, **107,** 013912.
29 J. Mao, Y. Sui, X. Zhang, Y. Su, X. Wang, Z. Liu, Y. Wang, R. Zhu, Y. Wang, W. Liu, J. Tang, *Appl. Phys. Lett*., 2011, **98,** 192510.
30 V. A. Khomchenko, I.O. Troyanchuk, R. Szymczak, H. Szymczak, *J. Mater. Sci.*, 2008, **43,** 5662.
31 J. Hemberger, S. Lobina , H.A. Krug von Nidda, N. Tristan, V.Y. Ivanov, A. A. Mukhin, A. M. Balbashov, A.Loidl, *Phys. Rev. B: Condens. Matter Mater. Phys.*, 2004, **70,** 024414.
32 I.O. Troyanchuk, V.A.Khomchenko, S.N. Pastushonok, O.A. Novitsky, V.I. Pavlov, H. Szymczak, *J. Magn. Magn. Mater*., 2006, **303,** 111.
33 K. Yoshii, A. Nakamura, Y. Ishii, Y. Mori, *J. Solid State Chem*., 2001, **162**, 84.
34 B. Rajeswaran, D.I. Khomskii, A.K. Zvezdin, C.N.R. Rao and A. Sundaresan, *Phys. Rev. B: Condens. Matter Mater. Phys.*, 2012, **86**, 214409.
35 A. Jaiswal, R. Das, K. Vivekanand, T. Maityand, P.M. Abraham, S. Adyanthaya, P. Poddar, *J. Appl. Phys.*, 2010, **107,** 013912.
36 P. Gupta, R. Bhargava, R. Das, P. Poddar, *RSC Adv*., 2013, **3,** 26427.
37 S. Niitaka, M. Azuma, M. Takano, E. Nishibori, M. Takata, M. Sakata, *Solid State Ionics*, 2004, **172,** 557.
38 T. Thangeeswari, J. Velmurugan, M. Priya, *J. Mater. Sci: Mater Electron*, 2013, **24**, 4817.
39 H-Y. Guo, J.I.L. Chen, and Z-G. Ye, *J. Mater. Res*., 2007, **22**, 8.
40 P. E. Wigen, A. Thavendrarajah, M. Pardavi-Horvath and M. Gomi，*Mat. Res. Soc.*, 1989, **150**.
41 B. Schulz and K. Baberschke, *Phys. Rev. B: Condens. Matter Mater. Phys.*, 1994, **50,** 13467.
42 T. M. Hong, *Phys. Rev. B: Condens. Matter Mater. Phys.*, 1998, **58**, 97.

